Journal of Physics D: Applied Physics

PAPER

Temperature dependent linewidth rebroadening in quantum dot semiconductor lasers

To cite this article: Felix Köster *et al* 2020 *J. Phys. D: Appl. Phys.* **53** 235106

IOP Publishing Journal of Physics D: Applied Physics
J. Phys. D: Appl. Phys. **53** (2020) 235106 (8pp) https://doi.org/10.1088/1361-6463/ab7ca5

Temperature dependent linewidth rebroadening in quantum dot semiconductor lasers

Felix Köster[1], Jianan Duan[2], Bozhang Dong[2], Heming Huang[2], Frédéric Grillot[2,3] and Kathy Lüdge[1]

[1] Institut für Theoretische Physik, Technische Universität Berlin, Berlin 10623 Germany
[2] LTCI, Télécom Paris, Institut polytechnique de Paris, 46 Rue Barrault, 75013 Paris, France
[3] Center for High Technology Materials,University of New-Mexico, Albuquerque, NM 87131 United States of America

E-mail: Felix-Koester@hotmail.com

Received 6 January 2020, revised 25 February 2020
Accepted for publication 4 March 2020
Published 8 April 2020

Abstract

We experimentally and analytically investigate the influence of temperature on the linewidth of an InP quantum dot (QD) laser. The full width half maximum of the peak in the optical spectrum strongly depends on the pump current and rebroadens at high injection levels. We show that with increasing temperature these effects are amplified. Applying a QD laser model including the excited and ground state with detailed balance scattering rates, we are capable of reproducing the experimentally observed data qualitatively and thus show that a relatively simple QD-laser model is capable of capturing this complex behavior. Additionally, we include a temperature dependent energy band gap reduction needed to fit the data and show that this effect enhances the rebroadening effect for higher temperatures.

Keywords: quantum dot lasers, solid state physics, linewidth

(Some figures may appear in colour only in the online journal)

1. Introduction

Since the invention of the laser in the 1950 s and its demonstration in 1960 it has been used for precise measurements because of the high spatial and spectral coherence. In particular, narrow line lasers has become an essential building-block of coherent communication systems and future LIDAR-based detection systems, in which phase noise strongly impacts the ratio of signal power to noise power [1, 2]. Semiconductor lasers with QDs have been especially of great interest [3, 4] with their low bias currents, high modulation bandwidths and their apparent temperature insensitivity, resulting from the highly confined carriers in the atomic-like electronic structure. QD lasers also have shown to exhibit emission linewidths of a few hundreds of kHz at room temperature[5, 6]. The spectral coherence of a laser can be measured via the linewidth, in which a smaller linewidth means a higher spectral coherence. The linewidth is influenced by the spontaneous emission, which on the one hand broadens the spectrum homogeneously through the lifetime of the carriers. On the other hand the spontaneous emission influences the linewidth via the amplitude-phase coupling [7], often approximately described via the α-factor [8]. The amplitude-phase coupling also depends on the inhomogeneity of the laser material, which is in QD lasers the self-organized growing technique, i.e. the epitaxial process, resulting in differently sized QDs [9]. For quantum well (QW) lasers measurements have shown that the α-factor is a more or less constant material parameter due to the linear dependence of both the refractive index and gain [10]. For a QD laser the description of gain and refractive index is more complex and also for the latter mainly non-resonant states contribute to this. These effects are called instantaneous frequency shifts [11–13]. The band structure of a QD laser contains localized energy levels. They are coupled via relative slow scattering rates and thus are not occupied through an equal distribution. The gain is consequently not clamped and the temperature and

the injection current influence the gain via the scattering rates as well as the refractive index α-factor. The usually defined α-factor is therefore non-constant in QD lasers and depends on the operation point. As a result, also the linewidth changes with the pump current [11, 14–17] and a linewidth rebroadening is observed for higher currents.

Previous work [15, 18] showed that this can be modeled by a minimal QD laser model, however, without capturing the effect of the temperature. In the following we investigate the influence of temperature on the linewidth rebroadening in a InP QD laser both by measurements, and via a QD laser model that contains the temperature via the detailed balance between in and out scattering rates. As a result the carrier distribution and thus the gain and the refractive index become temperature dependent. For the scattering we include carrier exchanges between the reservoir and the excited state (ES) and ground state (GS) and the relaxation rate between the two states [19]. The resulting non-linear scattering rates are based on microscopic calculations [19–21] and taken from [14]. We will show that the carrier temperature increases the linewidth and enhances the effect of rebroadening. We also included a temperature dependent band gap energy to reproduce measured shifts of the emitted wavelength and thus also of the level separations.

To calculate the linewidth a Gaussian white noise source is added to the complex electric field accounting for the spontaneous emission and the variance of the phase is thus derived by a semi-analytical approach through the variance matrix [22], where the Jacobian of the full system is evaluated at the steady state.

2. Studied device and experimental setup

The QD distributed feedback (DFB) lasers studied has a cavity length of 1 mm and a stripe width of 3 μm. The QD active region was grown by chemical beam epitaxy (CBE) on a (001) oriented n-type InP substrate, which contains 5 stacked layers of InAs QDs with 30 nm $In_{0.816}Ga_{0.184}As_{0.392}P_{0.608}$ (1.15Q) barriers. This active layer was embedded in a 350 nm thick 1.15Q waveguiding core resulting in both carrier and optical confinement. The QDs were tuned to operate in the desirable operation wavelength range by using a QD double cap growth procedure and a GaP sublayer. Growing the dots on a thin GaP layer allows a high dot density to be obtained and improved layer uniformity. An average dot density of approximately $4 \cdot 10^{10}$ cm^{-2} per layer was obtained, while a FWHM is found of 36.5 meV at 4 K which broadened to 60 meV at 300 K, indicating good dot size uniformity. After the growth of the QD active core, the wafer was removed to pattern the grating region which is performed by applying a HeCd laser to holographically expose an optical resist with a uniform grating pattern across the whole wafer, followed by wet chemical etching. Following the patterning of the grating, the p-type InP cladding and InGaAs contact layers were regrown using metal-organic chemical vapor deposition (MOCVD). The laser used a very low ($>0.01\%$) reflectivity antireflection coating on both facets in order to eliminate the termination phase of the grating at the cleaved facets.

In order to measure the spectral linewidth of the laser, we use a self-heterodyne fiber interferometer [5], where one part of the laser emission is sent to a 100 MHz frequency-shifted acousto-optic modulator (AOM) and another part propagates through a 25 km fiber coil. A polarization controller is also used to match the polarization between two parts. At the output of the interferometer the resulting beat note, centered at the AOM frequency, is recorded by an electrical spectrum analyzer through a high-speed photodiode. Two optical isolators providing 60 dB isolation were inserted just before the interferometer so as to eliminate the reflected light which introduces an optical feedback to the laser and affects the laser stability. In what follows, the measured spectra are curve-fitted by using the pseudo-Voigt approximation function which depends on a linear combination of Gaussian and Lorentzian functions.

3. Semiclassical single mode rate equation model

We use a QD laser model based on our previous work from [14] with a single optical mode which is resonant to the central GS transition. The carriers are described within an excitonic picture thus neglecting the separate degree of freedom for electrons and holes. The model originates from a semi-classical approach, meaning that the charge carriers are described microscopically, but the electric field classically with Maxwell's equations [23]. This model is able to describe the complex non-equilibrial carrier dynamics [24, 25]. Here we focus on the temperature dependent linewidth rebroadening. The excitonic band structure and the scattering processes are sketched in figure 1. We treat electrons and holes equally to simplify the calculations. The QD-laser system consists of the electrically pumped reservoir $N(t)$ which is filled to its quasi Fermi level $E_F(N)$, the two occupation probabilities of the carriers within the QD ρ_{ES} and ρ_{GS}, and the complex electric field $E(t) = A(t)e^{-i(\omega_L t+\Phi(t))}$, where $A(t)$ is the slowly varying amplitude within the rotating frame of the laser frequency ω_L. The total scattering contributions $R^{cap}_{ES/GS}$ and R^{rel} in equations (1)–(3) contain the temperature dependent in- and out scattering processes, which enables us to investigate the impact of the temperature T_{eq} on the linewidth rebroadening. The temperature dependent scattering rates also change the carrier distribution and thus the gain since there is no carrier clamping of the GS level. Secondly the refractive index and thus the effective α-factor of our device varies with temperature. Note that we describe the index shift by the linear relation $\delta\Omega N$. This has been derived from [12]. The ES is included in the carrier dynamics model and participates in the scattering processes but is not optically active. Stimulated emission can only occur from the GS. The equations are given by

$$\dot{N} = \eta J - \frac{N}{\tau_1} - 4N_{QD}R^{cap}_{ES} - 2N_{QD}R^{cap}_{GS} \tag{1}$$

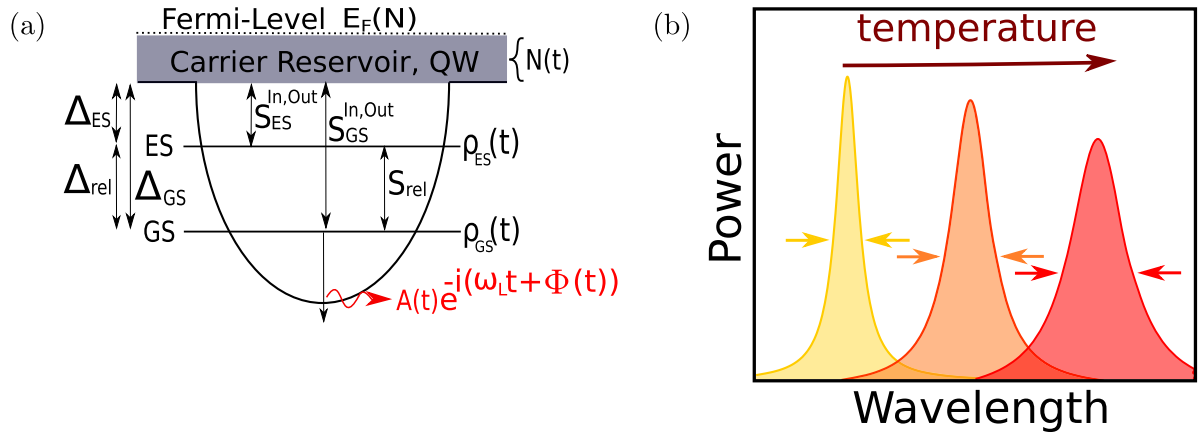

Figure 1. (a) Sketch of the bandstructure used for the QD laser model. ρ_{ES} and ρ_{GS} describe the probability occupations within the excited and ground state respectively within an excitonic picture, $N(t)$ is the charge carrier density in the reservoir acting as the charge carrier reservoir, which is electrically pumped. The emitted light $E(t)$ is described via its amplitude $A(t)$ within the rotating frame of the optical wavelength. $E(t) = A(t)e^{-i(\omega_L t+\Phi(t))}$. (b) Schematic Graph of the optical power spectrums for increasing temperature. The peak positions shift to higher wavelengths while the linewidth increases.

$$\dot{\rho}_{ES} = -\frac{\rho_{ES}}{\tau_{ES}} + R^{cap}_{ES} - \frac{1}{2}R^{rel} \tag{2}$$

$$\dot{\rho}_{GS} = -\frac{\rho_{GS}}{\tau_{GS}} + R^{cap}_{GS} + R^{rel} - g_0(2\rho_{GS}-1)A^2 \tag{3}$$

$$\dot{A} = \frac{1}{2}g_0(2\rho_{GS}-1)A - \frac{1}{2}\kappa A + D_{noise}\xi_A \tag{4}$$

$$\dot{\Phi} = -\delta\Omega N + \frac{D_{noise}}{A}\xi_\Phi. \tag{5}$$

The reservoir is pumped electrically by a current density J, which is normalized and non-dimensionalized to the elementary charge e and multiplied with the injection current efficiency factor η. The timescales τ_1, τ_{ES} and τ_{GS} describe the spontaneous recombination times of the reservoir charge carriers N, the ES charge carriers ρ_{ES} and the GS charge carriers ρ_{GS} respectively. The ES is twofold degenerated which explains the factor $\frac{1}{2}$ in equation (2). g_0 models the gain rate thus describing the Einstein coefficient, because A^2 is normalized such that it describes the photon number. κ models the photon losses and $\delta\Omega$ the change of instantaneous frequency due to refractive index changes. It describes the inhomogeneous linewidth enhancement resulting from non-resonant occupations. For $\delta\Omega = 0$ the laser is assumed to emit at ω_L. The value for $\delta\Omega$ was taken from [14] and slightly modified to fit the experimental data. We want to point out, that an explicit amplitude-phase coupling is excluded, as we want to show that the coupling via $\delta\Omega$ to the reservoir and the temperature dependent scattering rates are enough to qualitively describe the temperature dependent linewidth rebroadening. Because of the change of instantaneous frequency $\delta\Omega$ there is still an effective α-factor. R^{cap}_{ES}, R^{cap}_{GS} and R^{rel} describe the total scattering contributions from the reservoir N into the ES ρ_{ES} and GS ρ_{GS} and vice versa respectively and between the two states, which are defined as

$$R^{cap}_{ES/GS} = S^{cap,in}_{ES/GS}(1-\rho_{ES/GS}) - S^{cap,out}_{ES/GS}\rho_{ES/GS} \tag{6}$$

$$R^{rel} = S^{rel,in}(1-\rho_{GS})\rho_{ES} - S^{rel,out}\rho_{GS}(1-\rho_{ES}) \tag{7}$$

with $S^{cap,in}_{ES/GS}$, $S^{cap,out}_{ES/GS}$ being the in- and out-scattering rates from the reservoir into the ES or GS and $S^{rel,in}$, $S^{rel,out}$ being the in- and out-scatter rates from the ES into the GS. The relationship between the in- and out-scattering rates are given by the detailed balance relation $S^{cap,out}_{ES/GS} = f_{ES/GS}\cdot S^{cap,in}_{ES/GS}$ and $S^{rel,out} = \hat{f}\cdot S^{rel,in}$ with the corresponding Boltzmann factors $f_{ES/GS}(N), \hat{f}$ defined as [19, 26–28]

$$f_{ES/GS}(N) = \exp\left(\frac{-(E^F_{eq} - E_{ES/GS})}{k_B T_{eq}}\right) \tag{8}$$

$$\hat{f}(N) = \exp\left(\frac{-\Delta E_{rel}(T_{eq})}{k_B T_{eq}}\right). \tag{9}$$

Here, $E_{ES/GS}$ is the energy level of the ES and GS respectively, k_B is the Boltzmann constant and T_{eq} is the temperature of the QD charge carriers. We assume very fast scattering processes and thus a fast equalizing of the material's and the QD charge carrier's temperature. The E^F_{eq} is the quasi-Fermi level in the reservoir, which can be expressed in terms of the charge-carrier density in the reservoir by

$$E^F_{eq} = E^{res} + k_B T_{eq}\ln\left[\exp\left(\frac{N}{D_b k_B T_{eq}}\right) - 1\right]. \tag{10}$$

E^{res} is the reservoir band edge energy and D_b is the density of states within the reservoir. Substituting the quasi-Fermi level into equation (8) yields

$$f_{ES/GS}(N) = \frac{\exp\left(\frac{-\Delta E_{(ES,GS)}(T_{eq})}{k_B T_{eq}}\right)}{\exp\left(\frac{N}{D k_B T_{eq}}\right) - 1} \tag{11}$$

$$\hat{f}(N) = \exp\left(\frac{-\Delta E_{rel}(T_{eq})}{k_B T_{eq}}\right), \tag{12}$$

for the Boltzmann factors, where $\Delta E_{ES/GS}(T_{eq})$ is the energetic distance between the reservoir and the ES/GS and $\Delta E_{rel}(T_{eq})$ between the two states. We can thus rate the total scatter contribution as

$$R^{cap}_{ES/GS} = S^{cap,in}_{ES/GS}\left[1 - \rho_{ES/GS} - f_{ES/GS}\cdot\rho_{ES/GS}\right] \tag{13}$$

$$R^{rel} = S^{rel,in}\left[(1-\rho_{GS})\rho_{ES} - \hat{f}\cdot\rho_{GS}(1-\rho_{ES}))\right]. \tag{14}$$

The non-linear in-scattering rates $S^{cap,in}_{ES/GS}$ and $S^{rel,in}$ were taken from [14] and are given by

$$S^{cap,in}_{\rho_{ES}/\rho_{GS}}(N) = \frac{A_{ES/GS}\cdot N^2}{B_{ES/GS}+N} \tag{15}$$

$$S^{rel,in}(N) = \frac{C\cdot N}{D+N}, \tag{16}$$

where $A_{ES/GS}$,$B_{ES/GS}$,C and D are fit parameters derived from fits to the full microscopically calculated rates [29] of the electrons and holes. For our reduced model we use the average of the parameters fitted to the hole and electron scattering rates. We additionally included the temperature dependence of the band gap energies. This was done to reproduce the wavelength shifts to higher values with increasing temperature, which is shown schematically in figure 1(b). With this temperature dependent energy band we want to model all temperature influences resulting in wavelength shifts. The corresponding fit equation for the band gaps are given by

$$\Delta E_{(ES,GS)}(T_{eq}) = \Delta E_{(ES,GS)}(0) - \alpha\frac{T^2_{eq}}{T_{eq}+\beta} \tag{17}$$

$$\Delta E_{rel}(T_{eq}) = \Delta E_{rel}(0) - \alpha\frac{T^2_{eq}}{T_{eq}+\beta}, \tag{18}$$

where the corresponding fit parameters α and β of InP were taken from [30] and slightly modified because of the 1-D character of QDs. This was done by fitting the parameters to the measured wavelengths of the three different temperatures 293K, 303K and 313K, see figure 4. For simplicity the parameters are considered to be equal for the three band gap energies between reservoir and ES and GS and between the two states. These two effects make the Boltzmann factors $f_{ES/GS}$ and $\hat{f}$ the only temperature dependent quantities and thus relevant for the temperature dependent linewidth rebroadening.

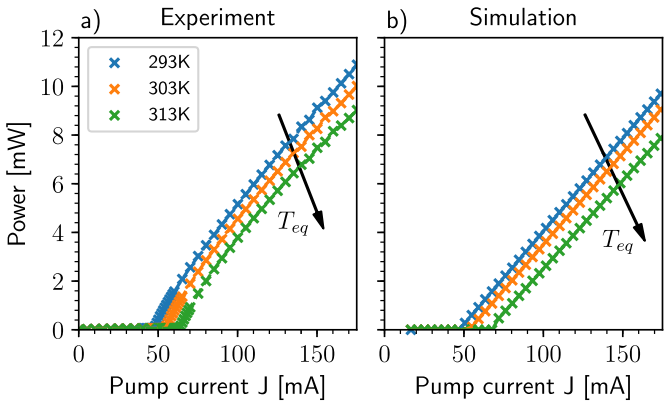

Figure 2. Input-output-curve: results of the (a) experiment and the (b) simulation of the output power of the laser for three different temperatures between 293K, 303K and 313K of the InP-QD laser plotted over the injection current J.A decrease in the output power can be seen for higher temperatures.

3.1. Analytics of linewidth calculation

Our analytical approach is based on a method known from stochastic differential equations [22], with which the variance $\underline{\underline{\sigma}}$ of a vector $\underline{x}$ given by a linear stochastic differential equation

$$\underline{dx} = \underline{\underline{A}}\cdot\underline{x}dt + \underline{\underline{B}}\cdot\underline{dW} \tag{19}$$

can be obtained via the covariance matrix $\underline{\underline{\sigma}}$ of the dynamical variables. It can be calculated via

$$\underline{\underline{\sigma}} = \int_0^t \exp\underline{\underline{A}}(t-t')\underline{\underline{B}}\underline{\underline{B}}^T\exp\underline{\underline{A}}^T(t-t')dt'. \tag{20}$$

If we linearize our QD laser model we arrive at a linear equation of the

$$\underline{dX} = \underline{\underline{A}}\cdot\underline{X}dt + \underline{\underline{B}}\cdot\underline{dW}, \tag{21}$$

with $X = (N, \rho_{ES}, \rho_{GS}, A, \Phi)$. $\underline{\underline{A}}$ is the Jacobian of the linearized system and $\underline{\underline{B}}$ is the noise matrix including the spontaneous emission of the complex electric field $D_{noise}\xi_A$ and $\frac{D_{noise}}{A}\xi_\Phi$ as Wiener processes (Gaussian white noise). The average variance of the phase $\sigma^2_{\Delta\Phi\Delta\Phi}$ in the long time limit then describes the linewidth of the laser via

$$\Delta\omega = \lim_{t\to\infty}\frac{1}{t}\sigma^2_{\Delta\Phi\Delta\Phi}(t). \tag{22}$$

We derive the Jacobian $\underline{\underline{A}}$ and the noise matrix $\underline{\underline{B}}$ analytically from equations (1)–(5) and use equation (20) to numerically calculate the variance matrix and then the linewidth via equation (22).

3.2. Comparison between experiment and theory

In this section we will compare the measurements to the numeric results from the model described in section 3. For this we set our focus on the output power of the laser, the spectrum

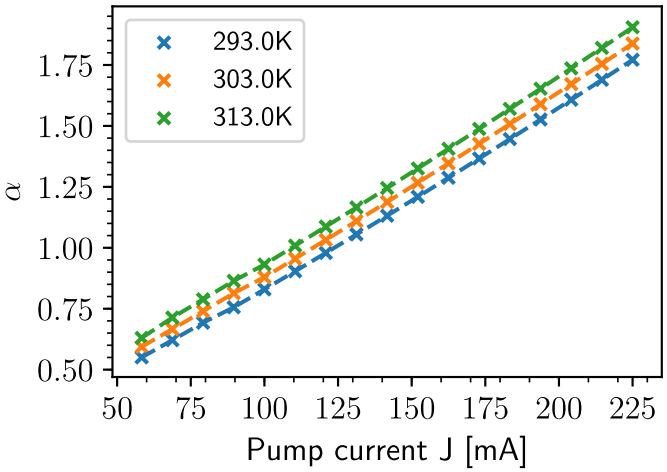

Figure 3. Calculated α-factors plotted over the pump current J for three different temperatures T_{eq}. The α-factor increases dynamically with the pump current J and the temperature.

and the temperature dependent linedwith rebroadening effect. All parameters that were used in the simulation are stated in table 1.

In figure 2 the light-current curve is plotted for the experiment (a) and the model (b) showing the output power over the injection current J. The light-current curves have been obtained for three different temperatures, e.g. 293K, 303K and 313K. Looking at figure 2(a), one can see a slight decrease in the output power for higher temperatures and a threshold shift to higher currents. This makes sense as higher temperatures, meaning higher thermal kinetic energy, results in more scattering processes out of the occupied states relative to the in-scatter processes and thus increasing the losses that have to be compensated by stimulated emission. This effect is also captured by the model as shown in figure 2(b). Mathematically this comes from equations (11) and (9) because higher temperatures increase the out-scattering rates. There is a slight difference in the quantitative value of the output power between experiment and theory which could be due to additional gain compression effects. Including these effects is possible but not needed to satisfactorily model the measured data of the linewidth rebroadening.

In order to show that the model intrinsically describes a temperature T_{eq} and pump current J dependent α-factor, we computed the effective α-factor over the pump current J for three different temperatures T_{eq}. Other papers have shown that the temperature dependent α-factor has an influence on the linewidth enhancement, which we show is included in this model [31]. This is shown in figure 3. The α-factor is hereby calculated via the relation $\alpha \propto \frac{\Delta\omega}{\Delta g}$, where $\Delta\omega$ is the difference of frequency and Δg the difference of gain for two operation points of the system, with one operation point calculated as a normal solution of the system and one operation point as a solution of the system with a small additional injection added to the electric field. The effective α-factor arises from the coupling between the phase Φ and the reservoir charge carriers N via the instantenous frequency shift $\delta\Omega$ even though the direct amplitude-phase coupling is excluded.

Table 1. Parameters used in the simulation if not stated otherwise.

Parameter	(Description)	Value (unit)
T_1	Lifetime of reservoir	1 ns^{-1}
T_{ES}	Lifetime of ES	0.75 ns^{-1}
T_{GS}	Lifetime of GS	0.75 ns^{-1}
2κ	Cavity loss rate	180.18 ns^{-1}
N_{QD}	QD density	$4 \cdot 10^{10}$ cm^{-2}
D	Density of states in reservoir	$6.26 \cdot 10^{32}$ cm^{-2}
ΔE_{ES}	Confinement for ES	64 meV
ΔE_{GS}	Confinement for GS	114 meV
ΔE_{rel}	Energetic distance between ES and GS	50 meV
g_0	Gain	350.285 ns^{-1}
A_{ES}	Parameter for Scat. rates ES	$5.6 \cdot 10^{-12}$ $cm^2 ns^{-1}$
B_{ES}	Parameter for Scat. rates ES	$1 \cdot 10^{11}$ cm^{-2}
A_{GS}	Parameter for Scat. rates GS	$7.25 \cdot 10^{-12}$ $cm^2 ns^{-1}$
B_{GS}	Parameter for Scat. rates GS	$3.6 \cdot 10^{11}$ cm^{-2}
C	Parameter for Scat. rates Rel.	520.65 ns^{-1}
D	Parameter for Scat. rates Rel.	$1.8 \cdot 10^{11}$ cm^{-2}
$\delta\Omega_N$	Reservoir carrier frequency shift	21 GHz
η	Injection current efficiency factor	0.25
D^2_{noise}	ES carrier frequency shift	8.55 KHz
α	Fit Parameter	$3.15 \cdot 10^{-4}$ eV K^{-1}
β	Fit Parameter	274 K

As mentioned in section 3 we use the measured wavelengths to fit our parameters α and β for capturing the temperature dependent wavelength shift. The wavelengths were measured at the peaks of the spectrum as shown in figure 4(a) and the results are plotted together with the measured wavelengths in figure 4(b). In figure 4(a) one can see a clear shift of the peaks to higher wavelengths for higher temperatures. This can be explained by the interplay between the amplitude phase coupling, i.e. the spontaneous frequency change $\delta\Omega$, and the temperature dependent energy band gap, which reduces the band gap energy with increasing temperature. With higher temperatures T_{eq} and a smaller band gap energy $\Delta E^{rel}_{ES/GS}$, out-scattering processes increase and with it the occupation of the reservoir charge carriers N. This increases the influence of the frequency change $\delta\Omega$ which then increases the effective α-factor. The variation of the phase Φ in equation (5) thus changes and the frequency of the electric field is increased. This corresponds to a smaller wavelength reducing the peak position in the power spectrum. In counterplay, smaller band gap energy $\Delta E^{rel}_{ES/GS}$ corresponds to a smaller emitting band gap frequency ω enhancing the emitted wavelength. Both effects are in the magnitude of a few meV. Taking both effects in consideration the peak wavelength can be calculated and has been plotted in figure 4(b). Fitting the temperature dependent band gap energy parameters reproduces the wavelengths of the experiment (orange cross) indicated by the blue line.

Reading out the FWHM at the emitted spectra one gets the linewidth of the QD-laser, which is usually done by fitting a Voigt profile to the peak [5]. This dependence of the linewidth

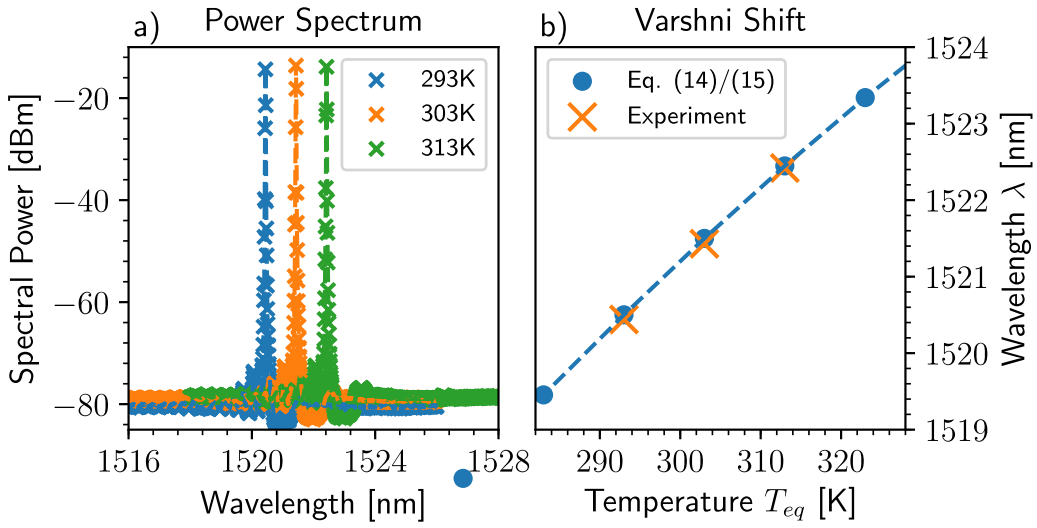

Figure 4. (a) Experimental measurements of the power spectrum for three different temperatures T_{eq}. An increase of T_{eq} shifts the wavelengths to higher values. (b) The peak wavelength position of the output power spectrum of the experiment (orange cross) and the model including the fit effect (blue line).

on the injection current J and the temperature T_{eq} is the main focus of this paper. Figures 5(a) and (b) show the measured and simulated linewidths $\Delta\omega$ respectively as a function of the pump current J in mA for three different temperatures, 293 K, 303 K and 313 K. The typical linewidth rebroadening is detectable for all temperatures [18]. See for example the green curve for 313K in figure 5(a). In [18] the rebroadening was explained by the gain compression effects. Note, that in this paper the gain compression is not a phenomenological parameter in equations (1)–(5) but results from the carrier dynamics within the complex gain model. For 293K the rebroadening effect can hardly be seen because the applied currents are not high enough. Comparing the different temperatures the influence of the thermal kinetic energy of the charge carriers is visible and leads to the higher linewidth. See the upshift of the curves in figure 5(a). The linewidth for 313K is higher for all J and the rebroadening effect starts at lower bias currents J and with an enhanced slope. Looking at the simulation results in figure 5(b) parts of this behavior is captured qualitatively. Higher temperatures result in higher linewidths, although the rebroadening slope is not increased for higher values of T_{eq}. Regarding equations (11) and (9) the influence of temperature should be clear when reformulating the Boltzmann factor and thus the factor that describes the out-scattering rates to

$$f_{ES/GS}(N) = \frac{\exp(a)}{\exp(b) - \exp(-\frac{1}{T_{eq}})},$$

with $a = \frac{-\Delta E_{(ES,GS)}}{k_B}$ and $b = \frac{N}{Dk_B}$. An increase in temperature increases the value of $\exp(-\frac{1}{T_{eq}})$, which enlarges the size of the whole fraction (Disregarding the possibility for negative values because $b = \frac{N}{Dk_B} > 0$, $T_{eq} > 0$.) and thus the whole term. The tempearture dependent energy band gap effect decreases $\Delta E_{ES/GS/rel}$ and thus also increases the out-scattering rates by a small amount. The same argument goes for the factor $\hat{f}_{ES/GS}(N)$ in equation (9). An intuitive explanation can be given by defining the quantity $\rho_{eq} = S_{ES/GS}^{cap/rel,in}/(S_{ES/GS}^{cap/rel,in} + S_{ES/GS}^{cap/rel,out})$, which describes the equilibrium occupation of the QD-level [32]. A higher value of ρ_{eq} stands for a higher equilibrium occupation reached via a higher percentage of in-scattering. In our model ρ_{eq} decreases with higher values of T_{eq} effectively reducing the relative in-scattering processes. As a result there are more charge carriers in the higher states ρ_{ES} and N which increases the instantaneous frequency change induced by $\delta\Omega$, and consequently also the variance of the phase $\sigma_{\Delta\Phi\Delta\Phi}$.

Without the detailed balance relation, i.e. the T-dependent Boltzmann factor between in an out scattering rates the simulated curves in figure 5 would be temperature independent.

Comparing the experimental data and the simulation, there are still discrepancies in the quantitative reproduction. For all three temperatures the rebroadening effect in the simulation occurs for similar injection currents J and with the same rebroadening slope. There are many effects, that could model this additional behavior. This could be due to missing temperature dependent effects, for example the joule heating of the device, the temperature dependent gain or considering the real temperature of the charge carriers, which can be higher. We excluded these effects here to keep the model as simple as possible, still able to reproduce the behavior of the experiment qualitively. Another point is that the temperature dependency was included in the detailed balance only and not in the in-scattering rates. It is known that the in-scattering rates are also temperature dependent [20, 33] and thus should have an additional influence on the temperature dependent linewidth rebroadening. Discrepancies could also be explained by missing hole burning effects and the separated treatment of electrons and holes. All these effects could be added to increase the accuracy of the model, but would only result in many parameters to tune the simulation until the outcome fits the desired measured values. This would be not in the sense of this paper.

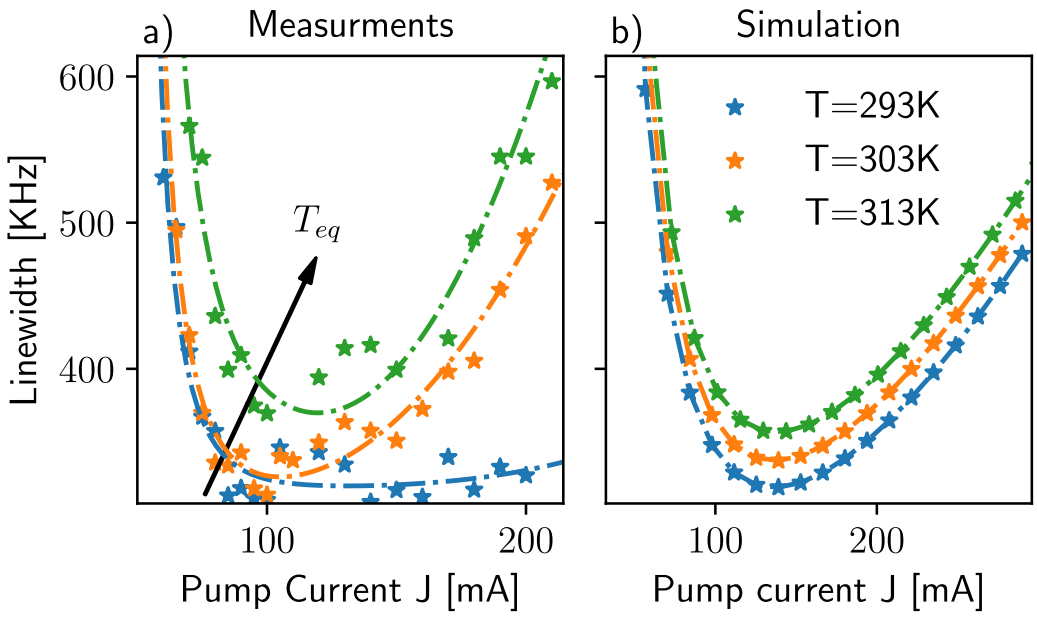

Figure 5. Results of the (a) experiment and the (b) simulation for the linewidth $\Delta\omega$ of the QD laser for three different temperatures, 293K, 303K and 313K plotted over the injection current. An increase in the linewidth rebroadening effect can be seen for higher temperatures.

4. Conclusion

With our model we have shown that the influence of temperature on the wavelength shift and the linewidth rebroadening in QD lasers, especially the pump current dependency, can be nicely described with a microscopically motivated model that includes the charge carrier dynamics within the surrounding reservoir and in the localized QD levels. A crucial ingredient is the correct description of in- and out-scattering processes via the temperature dependent detailed balance relation. Experimental data obtained on an InP based QD laser show the same trends and support our conclusion that the complex carrier dynamics is mainly responsible for the temperature sensitivity of the linewidth.

Acknowledgment

The authors would like to thank Philip J Poole and Zhenguo Lu from the Advanced Electronics and Photonics Research Centre, NRC Canada for providing the laser structures and Benjamin Lingnau for fruitful discussions. The authors also acknowledge the financial support by the "Deutscher Akademischer Austauschdienst" (DAAD), by the "Deutsche Forschungsgemeinschaft" (DFG) within SFB 787, and Campus France under the PhC Procope program (Grant 40 479YE).

ORCID iDs

Felix Köster https://orcid.org/0000-0002-3577-3690
Jianan Duan https://orcid.org/0000-0001-7710-4287
Bozhang Dong https://orcid.org/0000-0001-5826-6723
Frédéric Grillot https://orcid.org/0000-0001-8236-098X
Kathy Lüdge https://orcid.org/0000-0002-4831-8910

References

[1] Kikuchi K 2016 *IEEE J. Lightwave Technol.* **34** 157–79
[2] Lang X *et al* 2019 *Sci. China Info. Sci.* **62** 61401
[3] Coleman J J, Young J D and Garg A 2011 *IEEE J. Lightwave Technol.* **29** 499–510
[4] Chow W W and Jahnke F 2013 *Prog. Quantum Electron.* **37** 109–84
[5] Duan J, Huang H, Lu Z, Poole P, Wang C and Grillot F 2018 *Appl. Phys. Lett.* **112** 121102
[6] Becker A *et al* 2017 *Appl. Phys. Lett.* **110** 181103
[7] Chow W W and Koch S W 1999 *Semiconductor-Laser Fundamentals* (Berlin: Springer)
[8] Provost J G and Grillot F 2011 *IEEE Photonics Journal* **3** 476–88
[9] Bimberg D 2008 *Semiconductor Nanostructures* (Berlin: Springer)
[10] Henry C H 1982 *IEEE J. Quantum Electron.* **18** 259–64
[11] Lingnau B, Lüdge K, Chow W W and Schöll E 2012 *Phys. Rev.* E **86** 065201
[12] Lingnau B, Chow W W, Schöll E and Lüdge K 2013 *New J. Phys.* **15** 093031
[13] Osinski M and Buus J 1987 *IEEE J. Quantum Electron.* **23** 9–29
[14] Lingnau B, Chow W W and Lüdge K 2014 *Opt. Express* **22** 4867–79
[15] Melnik S, Huyet G and Uskov A V 2006 *Opt. Express* **14** 2950–5
[16] Gioannini M, Sevega A and Montrosset I 2006 Opt. Quantum Electron. **38** 381–94
[17] Grillot F, Dagens B, Provost J G, Su H and Lester L F 2008 *IEEE J. Quantum Electron.* **44** 946–51
[18] Redlich C, Lingnau B, Huang H, Raghunathan R, Schires K, Poole P J, Grillot F and Lüdge K 2017 *IEEE J. Sel. Top. Quantum Electron.* **23** 1901110
[19] Lüdge K and Schöll E 2009 *IEEE J. Quantum Electron.* **45** 1396–403
[20] Majer N 2012 Nonlinear gain dynamics of quantum dot semiconductor optical amplifiers *PhD Thesis*

[21] Lüdge K, Schöll E, Viktorov E A and Erneux T 2011 *J. Appl. Phys.* **109** 103112
[22] Gardiner C W 1985 *Handbook of Stochastic Methods* (Berlin: Springer)
[23] Haken H 1986 1st ed *Laser Light Dynamics* vol I (Amsterdam: North Holland)
[24] Erneux T and Glorieux P 2010 *Laser Dynamics* (Cambridge: Cambridge University Press)
[25] Chow W W and Koch S W 2005 *IEEE J. Quantum Electron.* **41** 495–505
[26] Lüdge K 2012 Modeling quantum dot based laser devices *Nonlinear Laser Dynamics - From Quantum Dots to Cryptography* (Weinheim: Wiley) ed Lüdge K ch 1 pp 3–34
[27] Meinecke S, Drzewietzki L, Weber C, Lingnau B, Breuer S and Lüdge K 2019 Sci. Rep. **9** 1783
[28] Lingnau B 2015 *Nonlinear and Nonequilibrium Dynamics of Quantum-Dot Optoelectronic Devices* (Cham: Springer)
[29] Majer N, Dommers-Völkel S, Gomis-Bresco J, Woggon U, Lüdge K and Schöll E 2011 *Appl. Phys. Lett.* **99** 131102
[30] Levinshtein M, Rumyantsev S and Shur M 1996 Ternary and quaternary A3B5 semiconductors *Handbook Series on Semiconductor Parameters* (Singapore: World Scientific)
[31] Septon T *et al* 2019 *Optica* **6** 1071–7
[32] Lingnau B and Lüdge K 2015 *Photonics* **2** 402–13
[33] Gomis-Bresco J, Dommers S, Temnov V V, Woggon U, Martinez-Pastor J, Lämmlin M and Bimberg D 2009 *IEEE J. Quantum Electron.* **45** 1121–8